



Modeling ultrafine
particle growth

Y. Y. Cui et al.

Modeling ultrafine particle growth at a pine forest site influenced by anthropogenic pollution during BEACHON-RoMBAS 2011

Y. Y. Cui¹, A. Hodzic², J. N. Smith^{2,7}, J. Ortega², J. Brioude^{3,4}, H. Matsui⁵,
A. Turnipseed², P. Winkler^{2,6}, and B. de Foy¹

¹Department of Earth and Atmospheric Sciences, Saint Louis University, MO 63108, USA

²National Center for Atmospheric Research, Atmospheric Chemistry Division, P.O. Box 3000, Boulder, CO 80307, USA

³Chemical Sciences Division, Earth System Research Laboratory, NOAA, Boulder, CO 80305, USA

⁴Cooperative Institute for Research in Environmental Sciences, University of Colorado, Boulder, CO 80309, USA

⁵Research Institute for Global Change, Japan Agency for Marine-Earth Science and Technology, Kanagawa, Japan

⁶Faculty of Physics, University of Vienna, Boltzmannngasse 5, 1090 Vienna, Austria

⁷Department of Applied Physics, University of Eastern Finland, 70211, Kuopio, Finland

Title Page

Abstract

Introduction

Conclusions

References

Tables

Figures

◀

▶

◀

▶

Back

Close

Full Screen / Esc

Printer-friendly Version

Interactive Discussion



Received: 6 February 2014 – Accepted: 24 February 2014 – Published: 4 March 2014

Correspondence to: A. Hodzic (alma@ucar.edu)

Published by Copernicus Publications on behalf of the European Geosciences Union.

ACPD

14, 5611–5651, 2014

Modeling ultrafine particle growth

Y. Y. Cui et al.

Title Page

Abstract

Introduction

Conclusions

References

Tables

Figures

◀

▶

◀

▶

Back

Close

Full Screen / Esc

Printer-friendly Version

Interactive Discussion



Abstract

Formation and growth of ultrafine particles is crudely represented in chemistry-climate models, which contributes to uncertainties in aerosol composition, size distribution, and aerosol effects on cloud condensation nuclei (CCN) concentrations. Measurements of ultrafine particles, their precursor gases, and meteorological parameters were performed in a ponderosa pine forest in the Colorado Front Range in July–August 2011, and were analyzed to study processes leading to Aitken-mode Particle burst Events (APEs). These measurements suggest that APEs were associated with the arrival at the site of anthropogenic pollution plumes around noon or in the early afternoon. Number concentrations of ultrafine (4 to 30 nm diameter) particles typically exceeded $10\,000\text{ cm}^{-3}$ during APEs, and these elevated concentrations coincided with increased SO_2 and monoterpene concentrations, and led to a factor of two increase in CCN concentrations at 0.5% supersaturation. The APEs were simulated using the regional WRF-Chem model, which was extended to account for ultrafine particle sizes starting at 1 nm in diameter, to include an empirical activation nucleation scheme in the planetary boundary layer, and to explicitly simulate the subsequent growth of Aitken particles by condensation of organic and inorganic vapors. Comparisons with aerosol size distribution measurements showed that simulations using the activation nucleation parameterization reasonably captured aerosol number concentrations and size distribution during APEs, as well as ground level CCN concentrations. Results suggest that sulfuric acid from anthropogenic SO_2 triggers APEs, and that the condensation of monoterpene oxidation products onto freshly nucleated particles drives their growth. The simulated growth rate of 3.4 nm h^{-1} for small particles (4–30 nm in diameter) was comparable to the measured average value of 2.3 nm h^{-1} . Model results also suggest that the presence of APEs tends to modify the composition of sub-100 nm diameter particles, leading to generally higher absolute mass concentrations of sulfate as well as organic aerosols with a higher sulfate content. Sensitivity simulations suggest that the representation of nucleation processes in the model largely influences the pre-

ACPD

14, 5611–5651, 2014

Modeling ultrafine particle growth

Y. Y. Cui et al.

Title Page

Abstract

Introduction

Conclusions

References

Tables

Figures

◀

▶

◀

▶

Back

Close

Full Screen / Esc

Printer-friendly Version

Interactive Discussion



dicted number concentrations and thus CCN concentrations. We estimate that nucleation contributes to 65 % of surface CCN at 0.5 % supersaturation in this pine forest environment.

1 Introduction

5 Submicron particles reduce atmospheric visibility, impact human health, and influence climate by radiative forcing and by modifying the number of cloud condensation nuclei (CCN) (Somers et al., 2004; Laaksonen et al., 2005). To accurately predict these effects, precise estimates of the aerosol size distribution are required (Adams and Seinfeld, 2002; Dusek et al., 2010) in addition to the typically-reported mass concentrations.

10 Modeling aerosol size distributions is challenging due to uncertainties involved in the formation and growth of new particles (Pierce et al., 2011). A new particle formation event is the result of a complex process where molecular clusters (1–2 nm) are created by nucleation of gases that may subsequently grow into detectable-sized particles depending on the outcome of two competing processes: condensation of semi-volatile

15 organic and inorganic gases and coagulation to preexisting particles (Kulmala, 2003; Kerminen and Kulmala, 2002; McMurry et al., 2005). Although mechanistic details of formation are still poorly understood, studies show that nucleated clusters originate from sulfuric acid, water, ammonia, and organic compounds (Zhang et al., 2004; Sipila et al., 2010; Kulmala et al., 2013; Kirkby et al., 2011). Ultrafine aerosols can become

20 active CCN with appropriate changes in their size distribution and chemical properties and thus can have an impact on cloud properties and precipitation (McFiggans et al., 2006). Pierce and Adams (2009) compared several nucleation schemes that spanned six orders of magnitude in globally averaged nucleation rates, and reported that the average tropospheric CCN concentrations varied by 17 % in the troposphere, and by

25 12 % within the boundary layer at low (0.2 %) supersaturations (SS). Kerminen et al. (2005) estimated that new particle formation over the boreal forests in Finland is asso-

Modeling ultrafine particle growth

Y. Y. Cui et al.

Title Page

Abstract

Introduction

Conclusions

References

Tables

Figures

◀

▶

◀

▶

Back

Close

Full Screen / Esc

Printer-friendly Version

Interactive Discussion



ciated with a radiative cooling of $0.2\text{--}0.9\text{ W m}^{-2}$ due to the effect of these particles on clouds.

The extent of the predicted nucleation event and its effect on CCN concentrations is largely dependent on the selected nucleation scheme and the environmental conditions. Previous studies have reported that binary and ternary homogeneous nucleation that is commonly used in 3-D models tends to underestimate nucleation rates and particle number concentrations by orders of magnitude, especially within the planetary boundary layer (PBL) (Kulmala et al., 2006; Young et al., 2008). Merikanto et al. (2009) used activation nucleation (AN) parameterization (Kulmala et al., 2006) in the boundary layer and binary homogeneous nucleation in the free troposphere, and estimated that nucleation contributes to 45 % of global mean CCN (0.2 % SS), of which 35 % can be attributed to the flux of nucleated particles from the free troposphere and 10 % from the boundary layer. Matsui et al. (2011) used a similar approach within the regional WRF-Chem model in the polluted urban environment of Beijing, and showed that new particle formation increased CCN concentrations at higher supersaturations ($> 0.2\%$ SS), and decreased CCN at lower supersaturation ($< 0.1\%$ SS). Luo and Yu (2011) used WRF-Chem and their Advanced Particle Microphysics model that includes the ion-mediated nucleation scheme and showed that new particle formation accounts for 80 % of CCN (0.4 % SS) in most parts of the Eastern United States.

In this paper, APEs at a semi-arid forest in the Colorado Front Range will be investigated from the 2011 BEACHON-RoMBAS field study. We use data from 25 July to 25 August 2011, to investigate the origin of aerosol formation and growth events, and to model their characteristics within the 3-D regional WRF-Chem model. The specific objectives of the study are: (1) to characterize APEs during the BEACHON-RoMBAS field campaign under the impact of anthropogenic pollution; and (2) to apply the activation nucleation parameterization in WRF-Chem to study APEs that occurred at the measurement site, and quantify their influences on ultrafine particles and CCN (0.5 % SS). As biogenic organic emissions dominate volatile organic compound concentrations at this site (Kaser et al., 2013; Ortega et al., 2014), we have also included their effects on

Modeling ultrafine particle growth

Y. Y. Cui et al.

Title Page

Abstract

Introduction

Conclusions

References

Tables

Figures

◀

▶

◀

▶

Back

Close

Full Screen / Esc

Printer-friendly Version

Interactive Discussion



the growth of newly nucleated particles in WRF-Chem. In this paper, we describe the circulation patterns at the MEFO site in Sect. 2, present our methods in Sect. 3, and discuss the results and conclusions of the two specific objectives in Sects. 4 and 5.

2 Measurement site and circulation patterns during the campaign

5 The Manitou Experimental Forest Observatory (MEFO; 39.1006° N, 105.0942° W) is located in the Front Range of the Colorado Rockies at 2300 m elevation in a subalpine forest dominated by ponderosa pine (Fig. 1). It is located 40 km northwest of Colorado Springs and 72 km southwest of Denver. The site is frequently influenced by polluted air from the Front Range urban areas. Previous studies at MEFO have indicated that
10 monoterpenes and 2-methyl-3-butene-2-ol (MBO) are the dominant component of VOC emissions during the daytime (Kim et al., 2010; Kaser et al., 2013; Ortega et al., 2014). The levels of anthropogenic pollutants (e.g. NO_x, SO₂, benzene) observed at the site are variable and driven by synoptic and local meteorological conditions. Observations of wind from the meteorological tower at MEFO have been used to analyze the diurnal variations of wind speeds and wind directions during the BEACHON-RoMBAS campaign
15 (Ortega et al., 2014). During daytime in the summer, easterly upslope flows are often observed at MEFO with wind speeds around 2–3 ms⁻¹, whereas during nighttime strong southwesterly drainage flows dominate with typical wind speeds around 3–5 ms⁻¹. An active Northern American Monsoon circulation influenced the measurement site from 25 July to 5 August, while the rest of the campaign period experienced
20 weak monsoon conditions with little precipitation.

Title Page

Abstract

Introduction

Conclusions

References

Tables

Figures

◀

▶

◀

▶

Back

Close

Full Screen / Esc

Printer-friendly Version

Interactive Discussion



3 Measurements and modeling framework

3.1 Datasets

Measurements from several instruments are used in this study to characterize APEs during BEACHON-RoMBAS 2011. Particle size distributions from 4 nm to 3 μm were measured on a 5 min cycle. The method consists of two Scanning Mobility Particle Sizers (SMPS) that measure particles from 4 nm to 30 nm and from 30 nm to 300 nm, and an optical particle counter that measures particles from 200 nm to 3 μm . The final data set is composed of the superposition of the 3 different measurements. The chemical composition of 20 nm diameter aerosol performed during BEACHON-RoMBAS is obtained by the Thermal Desorption Chemical Ionization Mass Spectrometer (TDCIMS, Voisin et al., 2003; Smith et al., 2004). During non-APE periods and during weak events (such as 8–11 August), the TDCIMS measured the composition of bulk aerosol ($< 1 \mu\text{m}$), whereas during APEs (such as 10 August) the instrument measured the composition of 20 nm diameter particles. The TDCIMS acquired data in “negative ion mode” using the reagent ion $\text{O}_2\text{-(H}_2\text{O)}_n$, where n is in the range of 1–3, which allows for the detection of inorganic and organic acids. Proton Transfer Reaction Quadrupole Mass Spectrometers (PTR-MS) with GC-MS analysis were used to measure monoterpenes. We also use gas-phase measurements of SO_2 and H_2SO_4 , meteorological measurements of wind speeds and direction, which were performed at 30 m above the surface, and measurements of CCN concentrations (most of the available data are at high supersaturation, equal or more than 0.5 % SS with critical activation diameter less than 65 nm, during this field campaign) and the corresponding derived hygroscopicity parameter, κ , for sub-100 nm particles (Petters and Kreidenweis, 2007). In this paper, the time is presented in Mountain Standard Time (MST).

The formation rate (J) and the growth rate are estimated from available measurements, starting at 4.4 nm diameter, and are used to constrain the model. To determine the formation rate of ~ 5 nm particles ($J_{5\text{nm}}$), we linearly fit the measured number concentrations of particles over the range of 4.4–6.25 nm diameter between the onset and

Title Page

Abstract

Introduction

Conclusions

References

Tables

Figures

◀

▶

◀

▶

Back

Close

Full Screen / Esc

Printer-friendly Version

Interactive Discussion



**Modeling ultrafine
particle growth**

Y. Y. Cui et al.

Title Page

Abstract

Introduction

Conclusions

References

Tables

Figures

◀

▶

◀

▶

Back

Close

Full Screen / Esc

Printer-friendly Version

Interactive Discussion



the end of APEs. The slope of the fitted line provides the measured formation rate ($J_{5\text{nm}}$) that is used to evaluate the model calculated formation rate for the model bin 3.98–6.31 nm. A similar method is applied to derive the formation rates for particles between 39–65 nm ($J_{50\text{nm}}$) and 101–162 nm ($J_{130\text{nm}}$) in the measurements, and their model equivalent values based on model bin 40–63 nm and bin 100–158 nm, respectively. It should be noted that the formation rate calculated here is the net formation rate which includes loss rates. We use the number mean diameter (NMD) to calculate the growth rate of particles in both measurements and simulations. Number mean diameter was defined by Matsui et al. (2011) using the diameter (nm) and number concentration (cm^{-3}) in each size bin. We use a linear fit to the values of NMD for particles smaller than 30 nm during APEs, and the slope of the fitted line is defined as the sub-30 nm growth rate. Additionally, we calculate the hygroscopicity parameter, Kappa, by including all aerosol species present in the model for particles smaller than 100 nm (see Sect. 4.4).

3.2 WRF-Chem simulations

Version 3.4.1 of the Weather Research and Forecasting model with chemistry (WRF-Chem) (Grell et al., 2005; Fast et al., 2006) was used with two nested domains over the continental United States. The grid resolution was 36 km for domain 1 and 4 km for domain 2 (Fig. 1). Two-way nesting was used between the domains. The WRF physics options chosen for our runs include the Monin–Obukhov scheme for the surface layer, the Yonsei University (YSU) scheme (Hong et al., 2006) for the planetary boundary layer, the Grell 3-D scheme (Grell and Devenyi, 2002) for the cumulus parameterization in the 36 km domain, the Lin et al. (1983) scheme for microphysics, the Rapid Radiative Transfer Model (Mlawer et al., 1997) for longwave radiation, and the Goddard scheme (Chou et al., 1998) for shortwave radiation. The nighttime minimum planetary boundary layer (PBL) height was set to 100 m in the YSU scheme to eliminate overestimating nocturnal concentrations of primary species. The land cover treatment was updated with MODIS land use data. North American Regional Reanalysis (NARR) data was

Modeling ultrafine particle growth

Y. Y. Cui et al.

Title Page

Abstract

Introduction

Conclusions

References

Tables

Figures

◀

▶

◀

▶

Back

Close

Full Screen / Esc

Printer-friendly Version

Interactive Discussion



used for the initial and boundary conditions at a 3 h temporal resolution and 32 km spatial resolution. Two representative periods were selected for our study: 25–30 July and 9–15 August. The first 24 h of each run were used to initialize the model, but were not used for comparisons. The meteorological outputs (such as wind field, PBL height, etc.) from WRF-Chem were used to drive a Lagrangian particle dispersion off-line model (see Sect. 3.3) to estimate the arrival of anthropogenic plumes at the MEFO site.

The chemistry is simulated using the CBMz gas-phase mechanism (Zaveri and Peters, 1999) and MOSAIC aerosol package (Zaveri et al., 2008). Similar to Matsui et al. (2011), we have modified the MOSAIC aerosol package in WRF-Chem v3.4.1 to explicitly account for a wider range of aerosol sizes, i.e., 20 bins over the aerosol diameter range from 1 nm to 10 μm . The default 8 bins over the range from 40 nm to 10 μm . The default binary homogenous nucleation scheme (Wexler et al., 1994) is used above the PBL, and it has been replaced by the empirical AN scheme within the PBL. The number concentration of nucleated clusters based on the empirical AN scheme is given by (Kulmala et al., 2006):

$$J^* = A \times \text{H}_2\text{SO}_4 \quad (1)$$

where J^* is the formation rate of activated clusters at 1 nm ($\text{cm}^{-3}\text{s}^{-1}$), A (s^{-1}) is the rate coefficient, and $[\text{H}_2\text{SO}_4]$ is the number concentration of gas-phase sulfuric acid (cm^{-3}). Previous studies indicate a large uncertainty associated with calculations of A , which was found to range between 10^{-5}s^{-1} and 10^{-8}s^{-1} (Kuang et al., 2008). The H_2SO_4 measurements are available from 9 to 26 August at MEFO and indicate that the average H_2SO_4 concentration is $\sim 2 \times 10^6$ molecules cm^{-3} during the late morning and noon. 28 July is the representative APE day during which particle sizes initiated at the smallest diameter during the RoMBAS observation period. We calculate the 5 nm aerosol formation rate ($J_{5\text{nm}}$; $\sim 1\text{cm}^{-3}\text{s}^{-1}$ as shown in Table 1) on that day, which results in a coefficient $A = 2 \times 10^{-6}\text{s}^{-1}$ that we used for the AN parameterizations in our simulations. It should be noted that here we only use values derived from measure-

Modeling ultrafine particle growth

Y. Y. Cui et al.

Title Page

Abstract

Introduction

Conclusions

References

Tables

Figures

◀

▶

◀

▶

Back

Close

Full Screen / Esc

Printer-friendly Version

Interactive Discussion



ments at MEFO to represent the AN parameterization of the model, and we simply use the observations in minimum particle size (~ 5 nm) to derive the formation of sub-5 nm diameter particles in AN parameterization. To simulate more accurately the growth of ultrafine particles, we included the condensation of semi-volatile oxidation products of isoprene, α -pinene and limonene onto pre-existing particles. The default model configuration only includes primary organic aerosols (Matsui et al., 2011), and accounting for the formation of secondary organic aerosols from biogenic emissions is key at this location as biogenic VOC emissions are significant. Simple molar yield calculations are used to form secondary organic aerosols, assuming 15 % contribution for α -pinene and limonene and 4 % for isoprene (Liu et al., 2012). To reduce the computational costs, the condensed mass is simply distributed in proportion to the aerosol surface area in each size bin. This simplification is consistent with other studies (Spracklen et al., 2006; Reddington et al., 2011) and assumes that the first generation oxidation products condense onto pre-existing particles with zero equilibrium vapor pressure.

Initial and boundary conditions for chemical species are provided by the MOZART-4 global chemistry-transport model (Emmons et al., 2010). For emissions, the EPA National Emission Inventory 2005 is used for the anthropogenic sources. The number size distribution of primary aerosol emissions was assumed to be a lognormal distribution with a median (peak) diameter of 50 nm and a standard deviation of 2.0. The MEGAN on-line model is applied for biogenic emissions (Guenther et al., 2006). Wet scavenging and dry deposition of gases and aerosols are also considered. The aerosol direct and indirect effects on radiation and cloud microphysics are included according to Gustafson et al. (2007) and Chapman et al. (2009).

Table 2 summarizes the WRF-Chem simulations and their characteristics. The base run (Ref-8bins) is the original WRF-Chem model with eight diameter bins starting at 40 nm. It includes the binary homogeneous nucleation parameterization in all vertical layers and does not account for the formation of secondary organic compounds (similar to Fast et al., 2009). The first test run (Nucleation-on) uses 20 bins and simulates the number concentration with the AN parameterization in the PBL and binary homo-

Modeling ultrafine particle growth

Y. Y. Cui et al.

Title Page

Abstract

Introduction

Conclusions

References

Tables

Figures

◀

▶

◀

▶

Back

Close

Full Screen / Esc

Printer-friendly Version

Interactive Discussion



geneous nucleation parameterization above the PBL. The second test run (Nucleation-
bsoa) is similar to Nucleation-on run but in addition it includes the condensation of bio-
genetic oxygenated semi-volatile organic compounds and their contribution to the growth
of ultrafine particles. A final sensitivity run (Nucleation-off) uses 20 bins and includes
5 the condensation of biogenic oxygenated semi-volatile organic compounds, but does
not include a nucleation parameterization (neither AN nor binary).

3.3 The trajectory model

To investigate the transport of anthropogenic air masses to the MEFO site during the
field study period, the Lagrangian particle dispersion model FLEXPART is used with
10 WRF (WRF-FLEXPART) (Stohl et al., 2005; Fast et al., 2006; Brioude et al., 2013).
The wind field used to drive FLEXPART is a time-averaged wind predicted by the
WRF-Chem 4 km simulations. We used the time-averaged wind to systematically de-
crease the uncertainty and bias in the trajectory calculations (Brioude et al., 2012).
In WRF-FLEXPART, the vertical diffusion coefficients were calculated based on the
15 the mixing heights and surface friction velocity from WRF-Chem. At the MEFO site, 10 000
inert tracer particles are released every hour at a random height between 50 and 100 m
above the ground. For each release, the backward trajectories are simulated for 48 h.
The total calculation time is 30 days from 27 July to 25 August 2013, and the number
of releases is 720. The hourly particle positions from the back trajectories are grid-
20 ded onto the 4 km × 4 km WRF-Chem domain to perform the Residence Time Analysis.
These gridded trajectories indicate the time that the air mass spent in each grid cell be-
fore arriving at MEFO (de Foy et al., 2007, 2008), which illustrates the preferred wind
directions and wind transport paths influencing the measurement site.

4 Results and discussion

4.1 Characterization of APE and Non-APE days

The temporal evolution of aerosol number size distributions observed during the entire campaign is shown in Fig. 2a. To distinguish between APE and Non-APE days, we calculate the ratio of the number concentrations of 4–30 nm particles ($N_{4-30\text{nm}}$) to the concentrations of 4–100 nm particles ($N_{4-100\text{nm}}$). If the ratio is larger than 0.5 (Jung et al., 2013) and the diurnal evolution of the aerosol number size distribution characterized by a banana-shaped plot (Dal Maso et al., 2005), then we consider that day to be an APE day. Using these criteria, we have selected four representative APEs (28, 29 July and 10, 13 August, see Fig. 2b), and three representative Non-APEs days (14, 23, and 24 August).

Figure 2b shows the observed temporal evolution of SO_2 mixing ratios and $N_{4-30\text{nm}}$ at MEFO during the campaign. $N_{4-30\text{nm}}$ appears to be highly correlated with SO_2 (Pearson correlation coefficient is 0.8), with $N_{4-30\text{nm}}$ peak values that systematically coincide with high SO_2 observed at the site. These results suggest that the inflow of anthropogenic pollutants impacts APEs at the MEFO site, and that the APEs are likely initiated by the products of SO_2 oxidation. The time evolution of monoterpenes (Fig. 2b) exhibits a more consistent day-to-day cycle with higher values at night, and lower values at the midday.

Observations of averaged diurnal profiles of SO_2 , monoterpenes, $N_{4-30\text{nm}}$, CCN (0.5 % SS), and number size distribution during four APE days and three Non-APE days also confirm these results (Fig. 3a–e). Significantly higher mean values are observed during APE days for both monoterpenes and SO_2 , and it is clear that $N_{4-30\text{nm}}$ is strongly increased starting midday during APE days (Fig. 3c). Measured CCN (0.5 % SS) number concentrations at the surface are also up to a factor of two higher during afternoon hours on APE days compared to Non-APE days (Fig. 3d). A sharp increase in CCN is observed in the afternoon, typically three hours after the start of APEs. There is also a large difference in size distributions between APE and Non-APE days for par-

[Title Page](#)[Abstract](#)[Introduction](#)[Conclusions](#)[References](#)[Tables](#)[Figures](#)[◀](#)[▶](#)[◀](#)[▶](#)[Back](#)[Close](#)[Full Screen / Esc](#)[Printer-friendly Version](#)[Interactive Discussion](#)

ticles smaller than 150 nm (Fig. 3e), which is typically the size range that encompasses the critical activation diameters for CCN (50–100 nm) (Petters and Kreidenweis, 2007). The peak of the number size distribution is shifted from ~ 110 nm on Non-APE days to smaller diameters ~ 30 nm on APE days.

To investigate the relationship between APEs and the transport of anthropogenic pollutants to the site, we have analyzed the origin of the air masses arriving at the measurement site prior to APEs. The wind roses measured at MEFO at a 30 m height show the variation of wind direction by time of day for APE and Non-APE days (Fig. 4a and b). During APE days, wind directions clearly show a shift from southwesterly in the early morning (06:00–09:00 MST) to easterly and then to south-easterly or north-easterly winds during the day (10:00–17:00 MST). The dominant easterly wind component indicates influence from the Front Range urban areas. On Non-APE days, there is no clear shift of the winds away from southwesterly in the afternoon. Because the measured near-surface winds at the site can be greatly influenced by local topography, we have performed the Residence Time Analysis based on the FLEXPART back-trajectories to confirm the origin of the air masses for the APE and Non-APE days. Figure 4c and d shows that on APE days air masses at MEFO came from the Colorado Springs area, whereas on Non-APE days the air masses are principally from the west. The results suggest that measured SO_2 at the MEFO site likely originated from industrial sources located in the Colorado Springs area. Consistent with measurements (Fig. 3), back-trajectory results emphasize the key role of anthropogenic pollutants in the occurrence of ultrafine particle events at the MEFO site.

Table 1 shows the observed and predicted growth rates, particle formation rates for ~ 5 nm, ~ 50 nm, and ~ 130 nm diameter particles, and number concentrations of particles in the 4–40 nm ($N_{4-40\text{nm}}$) and 40–100 nm ($N_{40-100\text{nm}}$) diameter ranges for APEs that occurred at MEFO on 28 and 29 July, and 10 August. The APEs at the MEFO site typically started around noon and early afternoon (10:20–15:00 MST), and occurred following easterly shifts in wind direction (Fig. 4a). Jung et al. (2013) compared APE burst time and particle number size distribution at an urban site and a forest site, and

Modeling ultrafine particle growth

Y. Y. Cui et al.

Title Page

Abstract

Introduction

Conclusions

References

Tables

Figures

◀

▶

◀

▶

Back

Close

Full Screen / Esc

Printer-friendly Version

Interactive Discussion



Modeling ultrafine particle growth

Y. Y. Cui et al.

Title Page

Abstract

Introduction

Conclusions

References

Tables

Figures

◀

▶

◀

▶

Back

Close

Full Screen / Esc

Printer-friendly Version

Interactive Discussion



found that late APE burst time and broader particle number size distributions were observed at the forest site than at the urban site. Figure S1 shows similar results for this study. These characteristics imply that several hours are needed for urban plumes to reach the site and that new particle formation is happening most likely hours away from the site. The dominance of non-local contributions to observed APEs at the site is further reinforced by the absence of particles smaller than 5 nm in the observed number size distributions. Especially in August (Fig. 7a), particles smaller than 10 nm were almost never observed, suggesting that nucleation likely occurred in upwind areas or in the free troposphere, and that nucleated particles had a few hours to grow before arriving at the measurement site (e.g., 10 August, Fig. 7a). On 13 August, an inverse banana-shaped growth is observed (Fig. 7). FLEXPART shows that this “shrinkage” in the observed number size distribution could be related to the change in the air mass that is being sampled over the site during this event. The arrival of a polluted air mass from the Colorado Springs area (which is closer than the Denver area) during the afternoon (see Fig. S2) is a likely reason for the appearance of smaller particles, which could have been nucleated slightly upwind of the measurement site.

$N_{4-40\text{nm}}$ and $N_{40-100\text{nm}}$ reported in Table 1 are calculated as average values over a two-hour time period following the peak of each APE. Here, we report particles from 4 to 40 nm instead of 4 to 30 nm in order to have a closer match with the corresponding bins in the simulations. The observed $N_{4-40\text{nm}}$ averaged during the event, varies from $\sim 16\,000$ to $\sim 28\,000\text{ cm}^{-3}$, and $N_{40-100\text{nm}}$ from $\sim 4\,000$ to $\sim 12\,000\text{ cm}^{-3}$. $N_{4-40\text{nm}}$ is three to four times higher compared to $N_{40-100\text{nm}}$. In addition, for all APEs, the average growth rate is 2.3 nm h^{-1} , and the average net rates of formation for $\sim 5\text{ nm}$, $\sim 50\text{ nm}$, and $\sim 130\text{ nm}$ particles are $0.74\text{ cm}^{-3}\text{ s}^{-1}$, $0.18\text{ cm}^{-3}\text{ s}^{-1}$, and $0.013\text{ cm}^{-3}\text{ s}^{-1}$, respectively. The values derived from these observations are consistent with previous results reported for other forested regions (Kuang et al., 2008; Westervelt et al., 2013). The comparisons between observations and simulations are discussed in the next section.

4.2 Evaluation of modeled APEs

The regional WRF-Chem model is used to simulate APEs and analyze interactions between anthropogenic and biogenic air masses, as well as the potential influence of APEs on CCN concentrations at the MEFO ground site. As mentioned in Sect. 3.2, the model includes both the AN parameterization that connects the anthropogenic SO₂ emissions to nucleation, and the contributions of biogenic VOC emissions to the growth of ultrafine particles. Comparisons with tower measurements suggest that WRF-Chem generally captures the temporal variability and the overall magnitudes of O₃, CO and NO₂ (Fig. S3) during APEs. Due to the complex mountain terrain, predicting the arrival of narrow pollution plumes at the site is challenging especially with the current model resolution of 4 km. For instance on 29 July, WRF-Chem did not capture the observed SO₂ plume at the site because of a west shift bias in the simulated wind direction. On 10 August, model-simulated SO₂ was lower than observations because of an excessively large westerly component in simulated winds. These biases in simulated SO₂ influence the predicted levels of H₂SO₄ and lead to model underestimation of APEs (e.g., $N_{4-40\text{nm}}$ in Figs. 6 and 7) on these days.

Given the challenges related to the modeling of the local meteorology, we first examine how the model is reproducing the average features observed during APE and Non-APE days. Figure 5a–f compares average diurnal profiles of observed and predicted parameters associated with number size distributions of Aitken mode particles. The comparison of the number concentrations shows a noticeable improvement in the model's ability to simulate the number size distributions when the Nucleation-bsoa run is used. The default WRF-Chem configuration (Ref-8bins) is not able to explicitly simulate $N_{4-40\text{nm}}$, and greatly underestimates (up to a factor of 4) the $N_{40-100\text{nm}}$ concentrations during both APE and Non-APE days. It also fails to reproduce the diurnal variations reported in measurements. On the other hand, the Nucleation-bsoa run captures well the increase in $N_{4-40\text{nm}}$ during APE days, although it has a tendency to nucleate some particles during Non-APE days as suggested by slightly overpredicted $N_{4-40\text{nm}}$

Title Page

Abstract

Introduction

Conclusions

References

Tables

Figures

◀

▶

◀

▶

Back

Close

Full Screen / Esc

Printer-friendly Version

Interactive Discussion



Modeling ultrafine particle growth

Y. Y. Cui et al.

[Title Page](#)[Abstract](#)[Introduction](#)[Conclusions](#)[References](#)[Tables](#)[Figures](#)[◀](#)[▶](#)[◀](#)[▶](#)[Back](#)[Close](#)[Full Screen / Esc](#)[Printer-friendly Version](#)[Interactive Discussion](#)

concentrations. Simulation results (Fig. 5e) are clearly improved in terms of number mean diameters (NMD). During APEs, the increase in number concentrations of ultrafine particles ($N_{4-40\text{nm}}$) leads to a drop in NMD at midday (12:00–18:00 MST) to values as low as ~ 30 nm, followed by an increase in NMD in the late afternoon due to the condensational growth of nucleated particles. As expected during APE days, the default Ref-8bins run did not capture the decrease in NMD during the early afternoon caused by the appearance of freshly nucleated particles. Observations (Fig. 3e) show that the peak of the number size distribution is shifted from ~ 110 nm on Non-APE days to smaller diameters ~ 30 nm on APE days. This shift in NMDs was well predicted by the Nucleation-bsoa run (Fig. S6). The comparison of modeled (Nucleation-bsoa) number size distributions between APE and Non-APE days shows the same shift in the peak diameter from ~ 100 nm on Non-APE days to ~ 40 nm on APE days (Fig. S6). During Non-APE days, the Nucleation-bsoa run predicts slightly better the observed evolution of NMD than Ref-8bins (Fig. 5f).

A more detailed day-to-day evaluation of predicted number concentrations and size distributions for Aitken mode particles is performed for 26–30 July (Fig. 6), and 10–14 August (Fig. 7). For this comparison, it is important to keep in mind that $N_{4-40\text{nm}}$ is controlled by regional scale nucleation and early particle growth, whereas $N_{40-100\text{nm}}$ is also influenced by regional transport and anthropogenic emissions. As mentioned in Sect. 4.1, during July APEs had a more typical banana-shaped size distribution and particles smaller than 5 nm were observed, suggesting that new-particle formation likely occurred close to the measurement site. During this period, modified WRF-Chem (Nucleation-bsoa run) is able to reproduce the banana shape of the number size distributions of these local APEs (Figs. 6a and b). The time series comparisons show that the “Nucleation-bsoa” simulation roughly captures the number concentrations variations for particle smaller than 40 nm (Fig. 6c) and the diurnal evolution of the number mean diameter (NMD) (Fig. 6e). The model however has a tendency to overpredict the number concentrations of larger $N_{40-100\text{nm}}$ particles and does not capture the sharp increase in those on 29 August.

Modeling ultrafine particle growth

Y. Y. Cui et al.

[Title Page](#)[Abstract](#)[Introduction](#)[Conclusions](#)[References](#)[Tables](#)[Figures](#)[◀](#)[▶](#)[◀](#)[▶](#)[Back](#)[Close](#)[Full Screen / Esc](#)[Printer-friendly Version](#)[Interactive Discussion](#)

During August, APEs were characterized by larger starting diameters (> 5 nm) suggesting that new-particles formation occurred upwind of the site or above the PBL and that already somewhat grown particles were transported to the site. During this period, WRF-Chem (Nucleation-bsoa run) initiated some local nucleation but did not grow these particles beyond 4 nm on 10, 11 and 14 August, and not beyond 8 nm on 12 August (Fig. 7a and b). The model results confirm that the sub-100 nm particles that are present at the site in both observations and predictions on these days were not locally generated through nucleation. A sensitivity simulation was performed for 10 August to investigate the contribution of local nucleation to modeled number concentrations (Fig. S4). In this simulation the binary nucleation parameterization was used above the PBL and no nucleation parameterization was used within the PBL. Model results from combined Nucleation-bsoa and sensitivity runs suggest that locally formed new particles were not able to grow enough to be observed, and that free-troposphere nucleated particles could have been mixed downward into the boundary layer and brought those newly formed larger particles (> 10 nm) to the surface. Also, the number size distribution is shifted towards larger diameters, suggesting that this could be a possible source of larger ultrafine particles found at the site during August. Furthermore, in order to quantify the importance of ultrafine particles advection to the site on 10 August, we run a case with nucleation turned off both in the PBL and above it. Under these conditions, no particles appear at the site, suggesting that the above-PBL nucleation contributes ultrafine particles (90 %) predicted at the surface, on this particular day.

On 13 August, the model starts nucleating particles locally but does not grow them until later in the afternoon (after 5 p.m. MST), when a small fraction of particles seems to grow to larger sizes. Local wind roses and back-trajectories (Fig. S2) both suggest a shift in wind direction from southwest to southeast during that afternoon, which advected polluted air from Colorado Springs to the measurement site as already discussed in Sect. 4.1. This change in air masses could have brought already nucleated ultrafine particles to the site, however the model shows that their sizes are larger than suggested by observations (Fig. 7b). As discussed below, this is consistent with the

model tendency to grow freshly nucleated particles faster than what was observed at the site.

Modeled 4–40 nm diameter growth rates, $J_{5\text{nm}}$, $J_{50\text{nm}}$, $J_{130\text{nm}}$ are shown in Table 1. In comparison with observations, we find that Nucleation-bsoa simulates comparable results but slightly overestimates the growth rates of particles up to 40 nm. For formation rates, Nucleation-bsoa underestimates small particles at 50 nm according to values of $J_{50\text{nm}}$ and overestimates particles larger than 100 nm as suggested by the comparison of $J_{130\text{nm}}$. Model calculations of $N_{4-40\text{nm}}$ and $N_{40-100\text{nm}}$ are comparable with observations, especially for $N_{40-100\text{nm}}$; however, $N_{4-40\text{nm}}$ on 29 July and 10 August are underestimated even in the Nucleation-bsoa run, especially on 10 August. Again, this indicates that the model configuration and spatial resolutions are not sufficiently accurate to capture all of the nucleation sources, and perhaps that the physical and chemical conditions that exist during nucleation events are not adequately represented by measurements performed at MEFO.

4.3 Sensitivity to the treatment of nucleation

There are large differences in simulation results in time series due to changes in the nucleation parameterizations (Figs. 6c–e and 7c–e). As already shown, the base case WRF-Chem simulation (Ref-8bins) does not explicitly simulate particles smaller than 40 nm, and shows large biases in both $N_{40-100\text{nm}}$ concentrations (Figs. 6c and 7c) and NMD (Figs. 6e and 7e) for both July and August. The number size distributions are not captured during the APE days suggesting that this base-case model version is not suitable for studying aerosol effect on CCN and clouds in forested environments. As expected, large differences from observations are found for the simulation that does not account for nucleation (nucleation-off run). This run under-predicts both $N_{4-40\text{nm}}$ and $N_{40-100\text{nm}}$ number concentrations by a factor of 5. Furthermore, it does not capture the low NMD periods and it overestimates the magnitude of NMDs by 2. Results from runs that include nucleation (nucleation-on run) generally overestimate $N_{4-40\text{nm}}$ except for 10 August, where the model tends to underestimate $N_{40-100\text{nm}}$. During July and Au-

Modeling ultrafine particle growth

Y. Y. Cui et al.

[Title Page](#)[Abstract](#)[Introduction](#)[Conclusions](#)[References](#)[Tables](#)[Figures](#)[◀](#)[▶](#)[◀](#)[▶](#)[Back](#)[Close](#)[Full Screen / Esc](#)[Printer-friendly Version](#)[Interactive Discussion](#)

Modeling ultrafine particle growth

Y. Y. Cui et al.

[Title Page](#)[Abstract](#)[Introduction](#)[Conclusions](#)[References](#)[Tables](#)[Figures](#)[◀](#)[▶](#)[◀](#)[▶](#)[Back](#)[Close](#)[Full Screen / Esc](#)[Printer-friendly Version](#)[Interactive Discussion](#)

gust, the model under-predicts the observed NMD by a factor of 2 suggesting that ultrafine particle growth is not sufficiently captured by the model. The comparison between Nucleation-on and Nucleation-bsoa runs allows quantifying the potential contribution of biogenic VOC to the growth of Aitken mode particles. Indeed, the Nucleation-bsoa run captures variations and magnitudes better compared to Nucleation-on that does not account for the formation of biogenic secondary organic aerosols (Sect. 3.2). The presence of biogenic secondary organic aerosol formation in the Nucleation-bsoa run results in a decrease of $N_{4-40\text{nm}}$, by almost an order of magnitude, and an increase in $N_{40-100\text{nm}}$ by a factor of two compared with Nucleation-on. Nucleation-bsoa better simulates $N_{40-100\text{nm}}$ during APE days but overestimates $N_{40-100\text{nm}}$ during Non-APE days. Overall, our results suggest that the condensational growth from semi-volatile organic compounds plays an important role in APEs over the Colorado Front Range, and that including the AN representation in the model considerably improves the simulation of APEs.

4.4 Composition of ultrafine particles during APEs and effects on CCN

TDCIMS measurements (see Sect. 3.1) show that freshly nucleated aerosols at MEFO are enriched in sulfate (Fig. 8a). A plot of the molar ratio, defined as the abundance of a specific ion divided by the sum of all ion abundances, of major species detected in 20 nm diameter particles during the APE on 10 August is shown in Fig. 8a. This is compared to measurements of bulk ($< 1\mu\text{m}$) aerosol composition averaged for 8, 9 and 11 August during Non-APE days (excludes the 10 August APE event). The plot shows a clear difference in the relative abundance of sulfate during the APE (63 %) vs. non-APE bulk aerosol (43 %). The Nucleation-bsoa run predicts the surface composition of small particles for various constituents, including sulfate, ammonium, nitrate, black carbon (BC), organic compounds, other inorganics (OIN), sodium, and chloride (here we show 4–20 nm particles, Fig. S5). On all days organic aerosols explain the majority, i.e., between 55 and 75 %, of the predicted mass. In addition, Fig. 8b show simulated results for the fractions of particles 4–20 nm during APEs days (28, 29 July

and 10 August) and non-APEs days (11 and 14 August). Results for APEs show a factor of two increase in the relative contribution of sulfate to aerosol mass concentrations relative to Non-APE days. In addition, for 4–20 nm particles, the Nucleation-bsoa run predicts much higher sulfate, ammonium, and organics than the Nucleation-off simulation, which illustrates the importance of nucleation processes in predictions of the ultrafine aerosol composition (see Fig. S5).

Changes in submicron particle composition during APEs can affect their hygroscopicity, and therefore modify their ability to form CCN. Here we compare the measured and predicted volume-averaged hygroscopicity parameter (κ) (Fig. 9). For calculations of κ in WRF-Chem, we consider typical hygroscopicity values (Chapman et al., 2009) shown in parentheses for individual compounds including sulfate (0.5), ammonium (0.5), nitrate (0.5), black carbon (10–6), organic compounds (0.14), other inorganics (OIN, 0.14), sodium (1.16), chloride (1.16). The calculated κ value is the average of the hygroscopicity of individual species weighted by their respective volume concentrations for aerosol sizes below 100 nm. For the Nucleation-bsoa run, the model reasonably simulates the measured values of κ . The Nucleation-bsoa simulation generally captures κ variability in the time series (Fig. 9a) except for the lowest observed values during the nighttime that are overestimated by the model. We should note that 29 July has very high values of κ (> 0.3) indicative of an increased contribution of sulfate aerosols during the APE event. The model does not reproduce those high values, at least in part because the simulations do not capture the SO_2 transport adequately on this day (see Sect. 4.2). The comparison of average diurnal profiles of observed and predicted κ values during APE and Non-APE days (Fig. 5g and h) shows that the Nucleation-bsoa run improves simulations of hygroscopicity compared to the model default simulation Ref-8bins. In both the Nucleation-bsoa run and measurements, κ values vary from ~ 0.05 to 0.2 during APE and Non-APE days, and these values are typically a factor of two lower than the default model simulation (Ref-8bins run) which does not account for the formation of secondary organic aerosols.

Modeling ultrafine particle growth

Y. Y. Cui et al.

Title Page

Abstract

Introduction

Conclusions

References

Tables

Figures

◀

▶

◀

▶

Back

Close

Full Screen / Esc

Printer-friendly Version

Interactive Discussion



Although Nucleation-bsoa simulates an increase in the afternoon values of Kappa that increase is not as pronounced as in the observations.

The time series of measured and simulated CCN (0.5 % SS) number concentrations are shown in Fig. 9c and d. In this study, CCN concentrations are treated explicitly, and small interstitial particles can be activated into CCN in the model. As CCN measurements were mainly performed at high supersaturation (Sect. 3.1), here we compare model results with CCN observations at 0.5 % SS. The Nucleation-bsoa run reasonably simulates the CCN (0.5 % SS) concentrations in both time series and diurnal profiles (Fig. 5) except on 29 July as expected. Figure 5i shows that the Nucleation-bsoa run captures the magnitudes of CCN (0.5 % SS) during the daytime, with however a slight underestimation of the afternoon values during APE days. The comparison of average diurnal profiles of CCN (0.5 % SS) shown in Fig. 5i also shows that the Nucleation-bsoa run simulates more accurately CCN (0.5 % SS) concentrations than the Ref-8bins run, especially during APE days. The Nucleation-off simulation underestimates by a factor of 3 the CCN (0.5 % SS) number concentration compared to Nucleation-bsoa (Fig. 9c and d). This indicates that the ability of the modified WRF-Chem to predict APES is dependent on including both AN nucleation parameterization and SOA formation. Comparing the results of Nucleation-bsoa with Nucleation-off during the two simulating periods, we find that the nucleation explains 67 % of near-surface CCN (0.5 % SS) concentrations at the MEFO site. This is an extreme case, however it illustrates that the accurate treatment of nucleation in 3-D models is important to predicting CCN (0.5 % SS) concentrations and aerosol number concentration in general.

5 Conclusions

Aitken-mode particle events (APEs), indicative of new particle formations and subsequent growth, were observed at the MEFO site during the 2011 BEACHON-RoMBAS field campaign. Four representative APEs were studied that showed a rapid increase in the number of 4–30 nm diameter particles from midday to early afternoon in this region.

Modeling ultrafine particle growth

Y. Y. Cui et al.

Title Page

Abstract

Introduction

Conclusions

References

Tables

Figures

◀

▶

◀

▶

Back

Close

Full Screen / Esc

Printer-friendly Version

Interactive Discussion



Modeling ultrafine particle growth

Y. Y. Cui et al.

[Title Page](#)[Abstract](#)[Introduction](#)[Conclusions](#)[References](#)[Tables](#)[Figures](#)[◀](#)[▶](#)[◀](#)[▶](#)[Back](#)[Close](#)[Full Screen / Esc](#)[Printer-friendly Version](#)[Interactive Discussion](#)

Number concentrations of 4 to 40 nm particles ranged from $\sim 16\,000$ to $28\,000\text{ cm}^{-3}$, and 40 to 100 nm particles ranged from $\sim 4\,000$ to $12\,000\text{ cm}^{-3}$. The average growth rate of 30 nm particles was 2.3 nm h^{-1} , and the average formation rates of $\sim 5\text{ nm}$, $\sim 50\text{ nm}$, and $\sim 130\text{ nm}$ diameter particles were $0.74\text{ cm}^{-3}\text{ s}^{-1}$, $0.18\text{ cm}^{-3}\text{ s}^{-1}$, and $0.013\text{ cm}^{-3}\text{ s}^{-1}$, respectively. The size distributions of ultrafine particles imply that non-local nucleation sources, including air masses originating above the PBL and upwind sources, impact MEFO. The diurnal profiles of SO_2 and monoterpene concentrations were investigated during APE and Non-APE days. Considerable differences between APEs and Non-APEs indicate that SO_2 plumes advected from the Colorado Front Range combined with biogenic monoterpenes significantly affect particle number concentrations and CCN during APEs.

A modified version of the WRF-Chem model was applied to study APEs during this campaign. The model was extended to include a parameterization of Activation Nucleation (AN) and the formation of SOA from biogenic and anthropogenic precursors. It also was used to simulate the corresponding volume-averaged hygroscopicity parameter (κ) and CCN concentrations. Comparisons with the un-modified WRF-Chem model (containing 8 particle diameter bins and binary homogeneous nucleation parameterization) indicate that AN parameterization more accurately simulates APEs in the 4–100 nm size range, including onset times, number concentrations and number mean diameters. The sensitivity simulations using the modified model without nucleation parameterization suggest that APEs influence the composition of small particles. Furthermore, the modified WRF-Chem simulations were able to represent variations and magnitudes of κ and number concentration of CCN (0.5 % SS), suggesting that the model can be used to study the connection between new particle formation and cloud formation. Our results from the enhanced WRF-Chem model highlighted the important role of the mixing of urban and forest air masses in the formation of APEs, and the value of the MEFO site in studying these events due to its location at the intersection of different air masses.

Acknowledgements. The authors would like to acknowledge data contributions, interesting discussions and editing from Lisa Kaser (University of Innsbruck, Austria), Ezra Levin (Colorado State University), David Gochis (National Center for Atmospheric Research, NCAR), Jerome Fast (Pacific Northwest National Laboratory, PNNL), and Christoph Knote (National Center for Atmospheric Research, NCAR). This research has been supported by the DOE DE-SC0006711 grant, and NCAR which is operated by the University Corporation for Atmospheric Research on behalf of the National Science Foundation. Authors would like to thank in particular the generous support of the NCAR's Advanced Study Program/Graduate Visitor Program. PMW acknowledges financial support from the Austrian Science Fund (FWF, Project No. J3198-N21). JNS acknowledges support from the National Science Foundation (ATM-0919317) and US Department of Energy (DE-SC0006861).

References

- Adams, P. J. and Seinfeld, J. H.: Predicting global aerosol size distributions in general circulation models, *J. Geophys. Res.*, 107, 4370, doi:10.1029/2001JD001010, 2002. 5614
- Brioude, J., Angevine, W. M., McKeen, S. A., and Hsie, E.-Y.: Numerical uncertainty at mesoscale in a Lagrangian model in complex terrain, *Geosci. Model Dev.*, 5, 1127–1136, doi:10.5194/gmd-5-1127-2012, 2012. 5621
- Brioude, J., Arnold, D., Stohl, A., Cassiani, M., Morton, D., Seibert, P., Angevine, W., Evan, S., Dingwell, A., Fast, J. D., Easter, R. C., Pisso, I., Burkhardt, J., and Wotawa, G.: The Lagrangian particle dispersion model FLEXPART-WRF version 3.1, *Geosci. Model Dev.*, 6, 1889–1904, doi:10.5194/gmd-6-1889-2013, 2013. 5621
- Chapman, E. G., Gustafson Jr., W. I., Easter, R. C., Barnard, J. C., Ghan, S. J., Pekour, M. S., and Fast, J. D.: Coupling aerosol-cloud-radiative processes in the WRF-Chem model: Investigating the radiative impact of elevated point sources, *Atmos. Chem. Phys.*, 9, 945–964, doi:10.5194/acp-9-945-2009, 2009. 5620, 5630

Modeling ultrafine particle growth

Y. Y. Cui et al.

Title Page

Abstract

Introduction

Conclusions

References

Tables

Figures

◀

▶

◀

▶

Back

Close

Full Screen / Esc

Printer-friendly Version

Interactive Discussion



Modeling ultrafine particle growth

Y. Y. Cui et al.

Title Page

Abstract

Introduction

Conclusions

References

Tables

Figures

◀

▶

◀

▶

Back

Close

Full Screen / Esc

Printer-friendly Version

Interactive Discussion



- Chou, M. D., Suarez, M. J., Ho, C. H., Yan, M. M. H., and Lee, K. T.: Parameterizations for cloud overlapping and shortwave single-scattering properties for use in general circulation and cloud ensemble models, *J. Climate*, 11, 202–214, 1998. 5618
- 5 Dal Maso, M., Kulmala, M., Riipinen, I., Wagner, R., Hussein, T., Aalto, P. P., and Lehtinen, K. E. J.: Formation and growth of fresh atmospheric aerosols: eight years of aerosol size distribution data from SMEAR II, Hyytiälä, Finland, *Boreal Environ. Res.*, 10, 323–336, 2005. 5622
- de Foy, B., Lei, W., Zavala, M., Volkamer, R., Samuelsson, J., Mellqvist, J., Galle, B., Martínez, A.-P., Grutter, M., Retama, A., and Molina, L. T.: Modelling constraints on the emission inventory and on vertical dispersion for CO and SO₂ in the Mexico City Metropolitan Area using Solar FTIR and zenith sky UV spectroscopy, *Atmos. Chem. Phys.*, 7, 781–801, doi:10.5194/acp-7-781-2007, 2007. 5621
- 10 de Foy, B., Fast, J. D., Paech, S. J., Phillips, D., Walters, J. T., Coulter, R. L., Martin, T. J., Pekour, M. S., Shaw, W. J., Kastendeuch, P. P., Marley, N. A., Retama, A., and Molina, L. T.: Basin-scale wind transport during the MILAGRO field campaign and comparison to climatology using cluster analysis, *Atmos. Chem. Phys.*, 8, 1209–1224, doi:10.5194/acp-8-1209-2008, 2008. 5621
- 15 Dusek, U., Frank, G. P., Curtius, J., Drewnick, F., Schneider, J., Kurten, A., Rose, D., Andreae, M. O., Borrmann, S., and Poschl, U.: Enhanced organic mass fraction and decreased hygroscopicity of cloud condensation nuclei (CCN) during new particle formation events, *Geophys. Res. Lett.*, 37, L03804, doi:10.1029/2009GL040930, 2010. 5614
- 20 Emmons, L. K., Apel, E. C., Lamarque, J.-F., Hess, P. G., Avery, M., Blake, D., Brune, W., Campos, T., Crawford, J., DeCarlo, P. F., Hall, S., Heikes, B., Holloway, J., Jimenez, J. L., Knapp, D. J., Kok, G., Mena-Carrasco, M., Olson, J., O’Sullivan, D., Sachse, G., Walega, J., Weibring, P., Weinheimer, A., and Wiedinmyer, C.: Impact of Mexico City emissions on regional air quality from MOZART-4 simulations, *Atmos. Chem. Phys.*, 10, 6195–6212, doi:10.5194/acp-10-6195-2010, 2010. 5620
- 25 Fast, J., Aiken, A. C., Allan, J., Alexander, L., Campos, T., Canagaratna, M. R., Chapman, E., DeCarlo, P. F., de Foy, B., Gaffney, J., de Gouw, J., Doran, J. C., Emmons, L., Hodzic, A., Herndon, S. C., Huey, G., Jayne, J. T., Jimenez, J. L., Kleinman, L., Kuster, W., Marley, N., Russell, L., Ochoa, C., Onasch, T. B., Pekour, M., Song, C., Ulbrich, I. M., Warneke, C., Welsh-Bon, D., Wiedinmyer, C., Worsnop, D. R., Yu, X.-Y., and Zaveri, R.: Evaluating simulated primary anthropogenic and biomass burning organic aerosols during MILAGRO: im-
- 30

Modeling ultrafine particle growth

Y. Y. Cui et al.

[Title Page](#)[Abstract](#)[Introduction](#)[Conclusions](#)[References](#)[Tables](#)[Figures](#)[◀](#)[▶](#)[◀](#)[▶](#)[Back](#)[Close](#)[Full Screen / Esc](#)[Printer-friendly Version](#)[Interactive Discussion](#)

plications for assessing treatments of secondary organic aerosols, *Atmos. Chem. Phys.*, 9, 6191–6215, doi:10.5194/acp-9-6191-2009, 2009. 5620

Fast, J. D., Gustafson, W., I., Jr., Easter, R. C., Zaveri, R. A., Barnard, J. C., Chapman, E. G., Grell, G. A., and Peckham, S. E.: Evolution of ozone, particulates, and aerosol direct radiative forcing in the vicinity of Houston using a fully coupled meteorology-chemistry-aerosol model, *J. Geophys. Res.-Atmos.*, 111, D21305, doi:10.1029/2005JD006721, 2006. 5618, 5621

Grell, G. A. and Devenyi, D.: A generalized approach to parameterizing convection combining ensemble and data assimilation techniques, *Geophys. Res. Lett.*, 29, 1693, doi:10.1029/2002GL015311, 2002. 5618

Grell, G. A., Peckham, S. E., Schmitz, R., McKeen, S. A., Frost, G., Skamarock, W. C., and Eder, B.: Fully coupled “online” chemistry within the WRF model, *Atmos. Environ.*, 39, 6957–6975, 2005. 5618

Guenther, A., Karl, T., Harley, P., Wiedinmyer, C., Palmer, P. I., and Geron, C.: Estimates of global terrestrial isoprene emissions using MEGAN (Model of Emissions of Gases and Aerosols from Nature), *Atmos. Chem. Phys.*, 6, 3181–3210, doi:10.5194/acp-6-3181-2006, 2006. 5620

Gustafson, W., I., Jr., Chapman, E. G., Ghan, S. J., Easter, R. C., and Fast, J. D.: Impact on modeled cloud characteristics due to simplified treatment of uniform cloud condensation nuclei during NEAQS 2004, *Geophys. Res. Lett.*, 34, L19809, doi:10.1029/2007GL030021, 2007. 5620

Hong, S. Y., Noh, Y., and Dudhia, J.: A new vertical diffusion package with an explicit treatment of entrainment processes, *Mon. Weather Rev.*, 134, 2318–2341, 2006. 5618

Jung, J., Miyazaki, Y., and Kawamura, K.: Different characteristics of new particle formation between urban and deciduous forest sites in Northern Japan during the summers of 2010–2011, *Atmos. Chem. Phys.*, 13, 51–68, doi:10.5194/acp-13-51-2013, 2013. 5622, 5623

Kaser, L., Karl, T., Schnitzhofer, R., Graus, M., Herdlinger-Blatt, I. S., DiGangi, J. P., Sive, B., Turnipseed, A., Hornbrook, R. S., Zheng, W., Flocke, F. M., Guenther, A., Keutsch, F. N., Apel, E., and Hansel, A.: Comparison of different real time VOC measurement techniques in a ponderosa pine forest, *Atmos. Chem. Phys.*, 13, 2893–2906, doi:10.5194/acp-13-2893-2013, 2013. 5615, 5616

Modeling ultrafine particle growth

Y. Y. Cui et al.

Title Page

Abstract

Introduction

Conclusions

References

Tables

Figures

◀

▶

◀

▶

Back

Close

Full Screen / Esc

Printer-friendly Version

Interactive Discussion



Kerminen, V. M. and Kulmala, M.: Analytical formulae connecting the “real” and the “apparent” nucleation rate and the nuclei number concentration for atmospheric nucleation events, *J. Aerosol Sci.*, 33, 609–622, 2002. 5614

Kerminen, V. -M., Lihavainen, H., Komppula, M., Viisanen, Y., and Kulmala, M.: Direct observational evidence linking atmospheric aerosol formation and cloud droplet activation, *Geophys. Res. Lett.*, 32, L14803, doi:10.1029/2005GL023130, 2005. 5614

Kim, S., Karl, T., Guenther, A., Tyndall, G., Orlando, J., Harley, P., Rasmussen, R., and Apel, E.: Emissions and ambient distributions of Biogenic Volatile Organic Compounds (BVOC) in a ponderosa pine ecosystem: interpretation of PTR-MS mass spectra, *Atmos. Chem. Phys.*, 10, 1759–1771, doi:10.5194/acp-10-1759-2010, 2010. 5616

Kirkby, J., Curtius, J., Almeida, J., Dunne, E., Duplissy, J., Ehrhart, S., Franchin, A., Gagne, S., Ickes, L., Kurten, A., Kupc, A., Metzger, A., Riccobono, F., Rondo, L., Schobesberger, S., Tsagkogeorgas, G., Wimmer, D., Amorim, A., Bianchi, F., Breitenlechner, M., David, A., Dommen, J., Downard, A., Ehn, M., Flagan, R. C., Haider, S., Hansel, A., Hauser, D., Jud, W., Junninen, H., Kreissl, F., Kvashin, A., Laaksonen, A., Lehtipalo, K., Lima, J., Lovejoy, E. R., Makhmutov, V., Mathot, S., Mikkila, J., Minginette, P., Mogo, S., Nieminen, T., Onnela, A., Pereira, P., Petaja, T., Schnitzhofer, R., Seinfeld, J. H., Sipila, M., Stozhkov, Y., Stratmann, F., Tome, A., Vanhanen, J., Viisanen, Y., Vrtala, A., Wagner, P. E., Walther, H., Weingartner, E., Wex, H., Winkler, P. M., Carslaw, K. S., Worsnop, D. R., Baltensperger, U., and Kulmala, M.: Role of sulphuric acid, ammonia and galactic cosmic rays in atmospheric aerosol nucleation, *Nature*, 476, 429–433, 2011. 5614

Kuang, C., McMurry, P. H., McCormick, A. V., and Eisele, F. L.: Dependence of nucleation rates on sulfuric acid vapor concentration in diverse atmospheric locations, *J. Geophys. Res.-Atmos.*, 113, D10209, doi:10.1029/2007JD009253, 2008. 5619, 5624

Kulmala, M.: How particles nucleate and grow, *Science*, 302, 1000–1001, 2003. 5614

Kulmala, M., Lehtinen, K. E. J., and Laaksonen, A.: Cluster activation theory as an explanation of the linear dependence between formation rate of 3 nm particles and sulphuric acid concentration, *Atmos. Chem. Phys.*, 6, 787–793, doi:10.5194/acp-6-787-2006, 2006. 5615, 5619

Kulmala, M., Kontkanen, J., Junninen, H., Lehtipalo, K., Manninen, H. E., Nieminen, T., Petaja, T., Sipila, M., Schobesberger, S., Rantala, P., Franchin, A., Jokinen, T., Jarvinen, E., Aijala, M., Kangasluoma, J., Hakala, J., Aalto, P. P., Paasonen, P., Mikkila, J., Vanhanen, J., Aalto, J., Hakola, H., Makkonen, U., Ruuskanen, T., Mauldin, R. L., Duplissy, J., Vehka-

Modeling ultrafine particle growth

Y. Y. Cui et al.

Title Page

Abstract

Introduction

Conclusions

References

Tables

Figures

◀

▶

◀

▶

Back

Close

Full Screen / Esc

Printer-friendly Version

Interactive Discussion



- maki, H., Back, J., Kortelainen, A., Riipinen, I., Kurten, T., Johnston, M. V., Smith, J. N., Ehn, M., Mentel, T. F., Lehtinen, K. E. J., Laaksonen, A., Kerminen, V. M., and Worsnop, D. R.: Direct Observations of Atmospheric Aerosol Nucleation, *Science*, 339, 943–946, 2013. 5614
- Laaksonen, A., Hamed, A., Joutsensaari, J., Hiltunen, L., Cavalli, F., Junkermann, W., Asmi, A., Fuzzi, S., and Facchini, M. C.: Cloud condensation nucleus production from nucleation events at a highly polluted region, *Geophys. Res. Lett.*, 32, L06812, doi:10.1029/2004GL022092, 2005. 5614
- Lin, Y.-L., Farley, R. D., and Orville, H. D.: Bulk parameterization of the snow field in a cloud model, *J. Climate Appl. Meteorol.*, 22, 1065–1092, 1983. 5618
- Liu, X., Easter, R. C., Ghan, S. J., Zaveri, R., Rasch, P., Shi, X., Lamarque, J.-F., Gettelman, A., Morrison, H., Vitt, F., Conley, A., Park, S., Neale, R., Hannay, C., Ekman, A. M. L., Hess, P., Mahowald, N., Collins, W., Iacono, M. J., Bretherton, C. S., Flanner, M. G., and Mitchell, D.: Toward a minimal representation of aerosols in climate models: description and evaluation in the Community Atmosphere Model CAM5, *Geosci. Model Dev.*, 5, 709–739, doi:10.5194/gmd-5-709-2012, 2012. 5620
- Luo, G. and Yu, F.: Simulation of particle formation and number concentration over the Eastern United States with the WRF-Chem + APM model, *Atmos. Chem. Phys.*, 11, 11521–11533, doi:10.5194/acp-11-11521-2011, 2011. 5615
- Matsui, H., Koike, M., Kondo, Y., Takegawa, N., Wiedensohler, A., Fast, J. D., and Zaveri, R. A.: Impact of new particle formation on the concentrations of aerosols and cloud condensation nuclei around Beijing, *J. Geophys. Res.-Atmos.*, 116, D19208, doi:10.1029/2011JD016025, 2011. 5615, 5618, 5619, 5620
- McFiggans, G., Artaxo, P., Baltensperger, U., Coe, H., Facchini, M. C., Feingold, G., Fuzzi, S., Gysel, M., Laaksonen, A., Lohmann, U., Mentel, T. F., Murphy, D. M., O'Dowd, C. D., Snider, J. R., and Weingartner, E.: The effect of physical and chemical aerosol properties on warm cloud droplet activation, *Atmos. Chem. Phys.*, 6, 2593–2649, doi:10.5194/acp-6-2593-2006, 2006. 5614
- McMurry, P. H., Fink, M., Sakurai, H., Stolzenburg, M. R., Mauldin, R. L., Smith, J., Eisele, F., Moore, K., Sjostedt, S., Tanner, D., Huey, L. G., Nowak, J. B., Edgerton, E., and Voisin, D.: A criterion for new particle formation in the sulfur-rich Atlanta atmosphere, *J. Geophys. Res.-Atmos.*, 110, D22S02, doi:10.1029/2005JD005901, 2005. 5614

Modeling ultrafine particle growth

Y. Y. Cui et al.

Title Page

Abstract

Introduction

Conclusions

References

Tables

Figures

◀

▶

◀

▶

Back

Close

Full Screen / Esc

Printer-friendly Version

Interactive Discussion



Merikanto, J., Spracklen, D. V., Mann, G. W., Pickering, S. J., and Carslaw, K. S.: Impact of nucleation on global CCN, *Atmos. Chem. Phys.*, 9, 8601–8616, doi:10.5194/acp-9-8601-2009, 2009. 5615

Mlawer, E. J., Taubman, S. J., Brown, P. D., Iacono, M. J., and Clough, S. A.: Radiative transfer for inhomogeneous atmospheres: RRTM, a validated correlated-k model for the longwave, *J. Geophys. Res.-Atmos.*, 102, 16663–16682, 1997. 5618

Ortega, J., Turnipseed, A., Guenther, A. B., Karl, T. G., Day, D. A., Gochis, D., Huffman, J. A., Prenni, A. J., Levin, E. J. T., Kreidenweis, S. M., DeMott, P. J., Tobo, Y., Patton, E. G., Hodzic, A., Cui, Y., Harley, P. C., Hornbrook, R. H., Apel, E. C., Monson, R. K., Eller, A. S. D., Greenberg, J. P., Barth, M., Campuzano-Jost, P., Palm, B. B., Jimenez, J. L., Aiken, A. C., Dubey, M. K., Geron, C., Offenberg, J., Ryan, M. G., Fornwalt, P. J., Pryor, S. C., Keutsch, F. N., DiGangi, J. P., Chan, A. W. H., Goldstein, A. H., Wolfe, G. M., Kim, S., Kaser, L., Schnitzhofer, R., Hansel, A., Cantrell, C. A., Mauldin III, R. L., and Smith, J. N.: Overview of the Manitou Experimental Forest Observatory: site description and selected science results from 2008–2013, *Atmos. Chem. Phys. Discuss.*, 14, 1647–1709, doi:10.5194/acpd-14-1647-2014, 2014. 5615, 5616

Petters, M. D. and Kreidenweis, S. M.: A single parameter representation of hygroscopic growth and cloud condensation nucleus activity, *Atmos. Chem. Phys.*, 7, 1961–1971, doi:10.5194/acp-7-1961-2007, 2007. 5617, 5623

Pierce, J. R. and Adams, P. J.: Uncertainty in global CCN concentrations from uncertain aerosol nucleation and primary emission rates, *Atmos. Chem. Phys.*, 9, 1339–1356, doi:10.5194/acp-9-1339-2009, 2009. 5614

Pierce, J. R., Riipinen, I., Kulmala, M., Ehn, M., Petäjä, T., Junninen, H., Worsnop, D. R., and Donahue, N. M.: Quantification of the volatility of secondary organic compounds in ultrafine particles during nucleation events, *Atmos. Chem. Phys.*, 11, 9019–9036, doi:10.5194/acp-11-9019-2011, 2011. 5614

Reddington, C. L., Carslaw, K. S., Spracklen, D. V., Frontoso, M. G., Collins, L., Merikanto, J., Minikin, A., Hamburger, T., Coe, H., Kulmala, M., Aalto, P., Flentje, H., Plass-Dülmer, C., Birmili, W., Wiedensohler, A., Wehner, B., Tuch, T., Sonntag, A., O'Dowd, C. D., Jennings, S. G., Dupuy, R., Baltensperger, U., Weingartner, E., Hansson, H.-C., Tunved, P., Laj, P., Sellegrì, K., Boulon, J., Putaud, J.-P., Gruening, C., Swietlicki, E., Roldin, P., Henzing, J. S., Moerman, M., Mihalopoulos, N., Kouvarakis, G., Ždímal, V., Zíková, N., Marinoni, A., Bonasoni, P., and Duchi, R.: Primary versus secondary contributions to particle number concentrations in

Modeling ultrafine particle growth

Y. Y. Cui et al.

[Title Page](#)[Abstract](#)[Introduction](#)[Conclusions](#)[References](#)[Tables](#)[Figures](#)[◀](#)[▶](#)[◀](#)[▶](#)[Back](#)[Close](#)[Full Screen / Esc](#)[Printer-friendly Version](#)[Interactive Discussion](#)

the European boundary layer, *Atmos. Chem. Phys.*, 11, 12007–12036, doi:10.5194/acp-11-12007-2011, 2011. 5620

Sipila, M., Berndt, T., Petaja, T., Brus, D., Vanhanen, J., Stratmann, F., Patokoski, J., Mauldin, R., L., III., Hyvarinen, A.-P., Lihavainen, H., and Kulmala, M.: The role of sulfuric acid in atmospheric nucleation, *Science*, 327, 1243–1246, 2010. 5614

Somers, C. M., McCarry, B. E., Malek, F., and Quinn, J. S.: Reduction of particulate air pollution lowers the risk of heritable mutations in mice, *Science*, 304, 1008–1010, 2004. 5614

Spracklen, D. V., Carslaw, K. S., Kulmala, M., Kerminen, V.-M., Mann, G. W., and Sihto, S.-L.: The contribution of boundary layer nucleation events to total particle concentrations on regional and global scales, *Atmos. Chem. Phys.*, 6, 5631–5648, doi:10.5194/acp-6-5631-2006, 2006. 5620

Stohl, A., Forster, C., Frank, A., Seibert, P., and Wotawa, G.: Technical note: The Lagrangian particle dispersion model FLEXPART version 6.2, *Atmos. Chem. Phys.*, 5, 2461–2474, doi:10.5194/acp-5-2461-2005, 2005. 5621

Westervelt, D. M., Pierce, J. R., Riipinen, I., Trivitayanurak, W., Hamed, A., Kulmala, M., Laaksonen, A., Decesari, S., and Adams, P. J.: Formation and growth of nucleated particles into cloud condensation nuclei: model–measurement comparison, *Atmos. Chem. Phys.*, 13, 7645–7663, doi:10.5194/acp-13-7645-2013, 2013. 5624

Wexler, A. S., Lurmann, F. W., and Seinfeld, J. H.: Modeling urban and regional aerosols, I. Model development, *Atmos. Environ.*, 28, 531–546, 1994. 5619

Young, L. H., Benson, D. R., Kameel, F. R., Pierce, J. R., Junninen, H., Kulmala, M., and Lee, S.-H.: Laboratory studies of H₂SO₄/H₂O binary homogeneous nucleation from the SO₂ + OH reaction: evaluation of the experimental setup and preliminary results, *Atmos. Chem. Phys.*, 8, 4997–5016, doi:10.5194/acp-8-4997-2008, 2008. 5615

Zaveri, R. A. and Peters, L. K.: A new lumped structure photochemical mechanism for large-scale applications, *J. Geophys. Res.-Atmos.*, 104, 30387–30415, 1999. 5619

Zaveri, R. A., Easter, R. C., Fast, J. D., and Peters, L. K.: Model for Simulating Aerosol Interactions and Chemistry (MOSAIC), *J. Geophys. Res.-Atmos.*, 113, D13204, doi:10.1029/2007JD008782, 2008. 5619

Zhang, R. Y., Suh, I., Zhao, J., Zhang, D., Fortner, E. C., Tie, X. X., Molina, L. T., and Molina, M. J.: Atmospheric new particle formation enhanced by organic acids, *Science*, 304, 1487–1490, 2004. 5614

Modeling ultrafine particle growth

Y. Y. Cui et al.

Table 1. Characteristics of four representative APEs at the MEFO site during the BEACHON-RoMBAS-2011 field campaign. Metrics are reported for observations and the WRF-Chem model simulations (Nucleation-bsoa). It is noted that: (1) Growth rate of ultrafine particles from 4 to 40 nm, in nm h^{-1} . (2) J : formation rate of small particles ~ 5 nm, ~ 50 nm and ~ 130 nm, in $\text{cm}^{-3} \text{s}^{-1}$. (3) Number concentration of particles at 4–40 nm and 40–100 nm, in number cm^{-3} . The mean values are averaged over a two-hour time period following the peak of each APE. In the model, values from bins #4 to #8 (from 3.98 to 39.8 nm), and from bins #9 and #10 (from 39.8 to 100 nm) are evaluated using observed $N_{4-40\text{nm}}$ and $N_{40-100\text{nm}}$.

APEs (< 30 nm) burst time (MST)		Growth rate	$J_{5\text{nm}}$	$J_{50\text{nm}}$	$J_{130\text{nm}}$	$N_{4-40\text{nm}}$ max	mean	$N_{40-100\text{nm}}$ max	mean
07–28 10:20	Obs	2.5	0.74	0.21	0.01	20 540	16 155	4160	3795
	Model	3.0	1.09	0.20	0.02	34 440	31 515	5389	5357
07–29 12:25	Obs	2.0	NaN	0.24	0.02	31 710	27 865	13 410	11 622
	Model	3.7	NaN	0.11	0.03	10 650	9551	5342	5282
08–10 10:20	Obs	2.5	NaN	0.08	0.01	22 000	21 470	6562	5336
	Model	NaN	NaN	0.02	0.004	3055	2968	5321	5178
Average	Obs	2.3	0.74	0.18	0.013				
	Model	3.4	1.09	0.11	0.018				

Title Page

Abstract Introduction

Conclusions References

Tables Figures

◀ ▶

◀ ▶

Back Close

Full Screen / Esc

Printer-friendly Version

Interactive Discussion



Modeling ultrafine particle growth

Y. Y. Cui et al.

Table 2. Description of model simulations. AN is activation nucleation parameterization, and BHN is binary homogeneous nucleation parameterization, which is the default option in the WRF-Chem model (see Sects. 1 and 3.2).

Simulations	Number of aerosol bins	Nucleation parameterizations		Accounting for condensation of biogenic VOCs
		Within PBL	Above PBL	
Ref_8bins	8 bins (40 nm–10 μ m)	BHN	BHN	No
Nucleation-on	20 bins (1 nm–10 μ m)	AN	BHN	No
Nucleation-bsoa	20 bins (1 nm–10 μ m)	AN	BHN	Yes
Nucleation-off	20 bins (1 nm–10 μ m)	None	None	Yes

Title Page

Abstract

Introduction

Conclusions

References

Tables

Figures

◀

▶

◀

▶

Back

Close

Full Screen / Esc

Printer-friendly Version

Interactive Discussion



Modeling ultrafine particle growth

Y. Y. Cui et al.

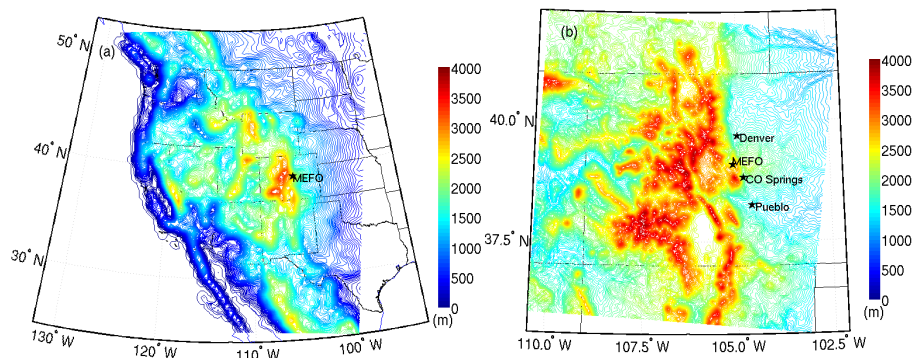


Fig. 1. WRF-Chem domains. **(a)** Coarse domain covers the western US with $36\text{ km} \times 36\text{ km}$ horizontal resolution, **(b)** Nested domain covers Colorado with $4\text{ km} \times 4\text{ km}$ resolution. Maps also show the topography, and the locations of the MEFO site, Denver, Colorado Springs, and Pueblo.

[Title Page](#)[Abstract](#)[Introduction](#)[Conclusions](#)[References](#)[Tables](#)[Figures](#)[◀](#)[▶](#)[◀](#)[▶](#)[Back](#)[Close](#)[Full Screen / Esc](#)[Printer-friendly Version](#)[Interactive Discussion](#)

Modeling ultrafine particle growth

Y. Y. Cui et al.

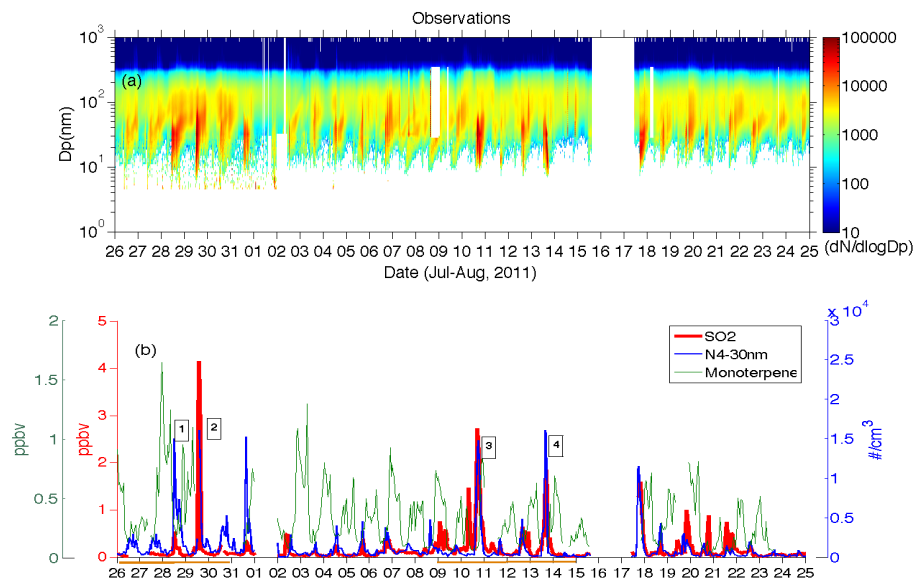


Fig. 2. (a) Time series of number size distribution of submicron particles during BEACHON-RoMBAS. (b) Temporal variations in number concentrations of 4–30 nm diameter particles ($N_{4-30\text{nm}}$) (blue), SO_2 (red), and monoterpene (green) mixing ratios during the campaign. The four APEs are selected (28 July and 29, and 10 August and 13) for comparisons with the model. The orange lines indicate simulation periods considered in the WRF-Chem model.

Title Page

Abstract

Introduction

Conclusions

References

Tables

Figures

◀

▶

◀

▶

Back

Close

Full Screen / Esc

Printer-friendly Version

Interactive Discussion



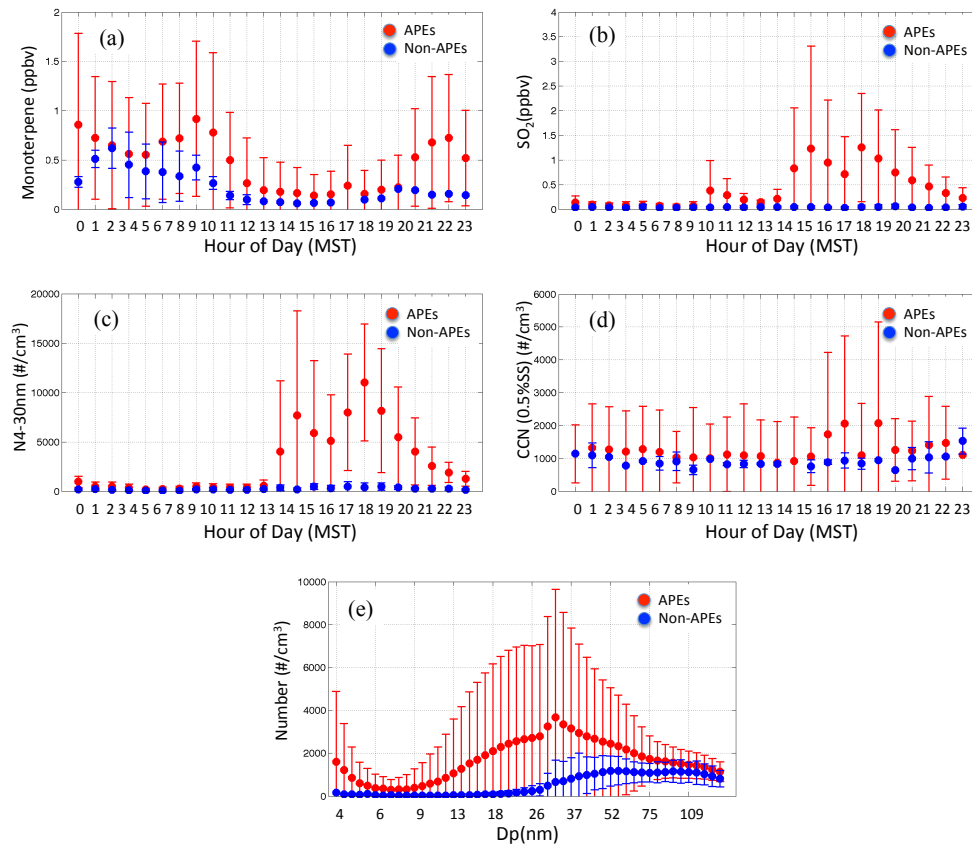


Fig. 3. Hourly averaged diurnal profiles of **(a)** monoterpenes, **(b)** SO₂ and **(c)** number concentrations of 4–30 nm diameter particles during APEs and non-APEs, respectively. **(d)** Hourly averaged CCN concentrations at 0.5% supersaturation for APEs and non-APEs. **(e)** Number size distribution (from 4.4–150 nm) during APEs and non-APEs. Error bars indicate 1σ variability.

Modeling ultrafine particle growth

Y. Y. Cui et al.

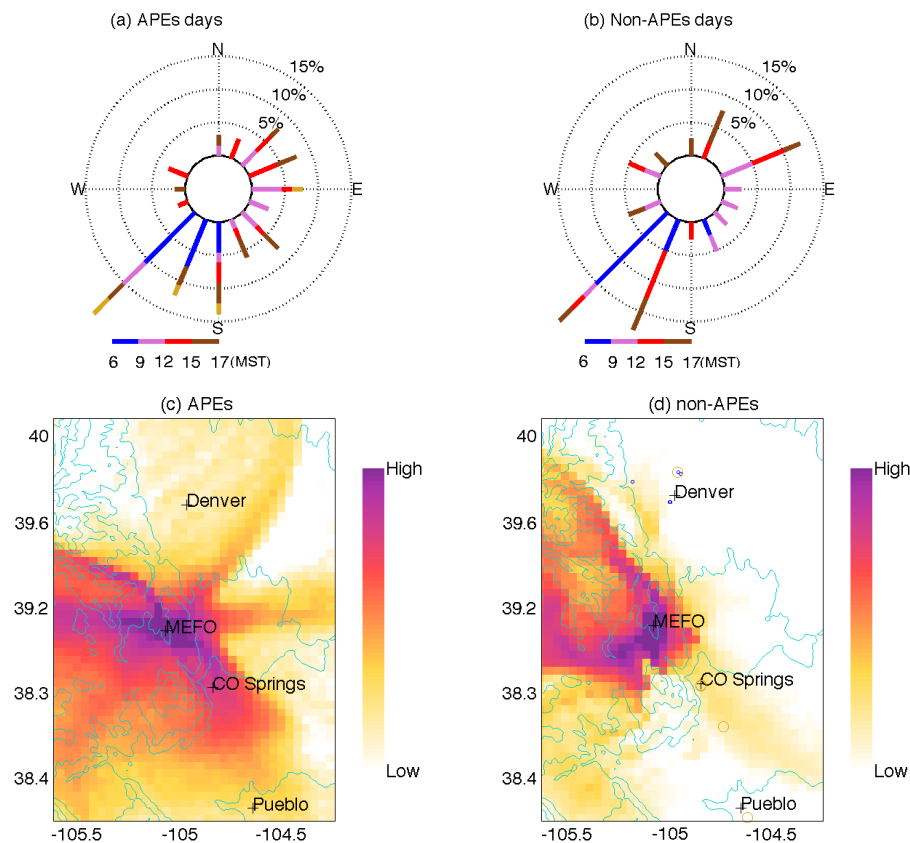
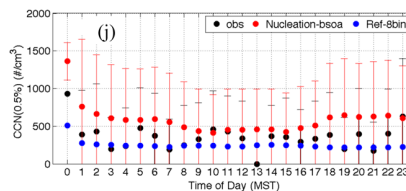
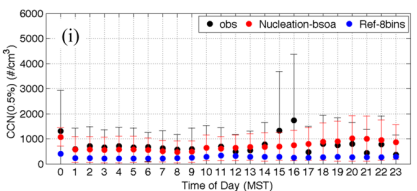
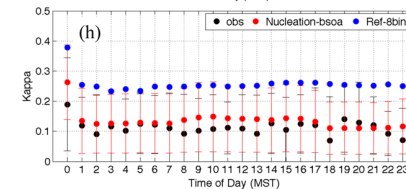
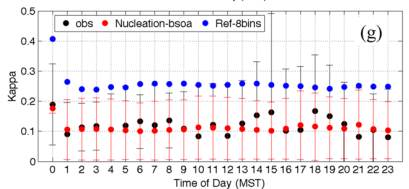
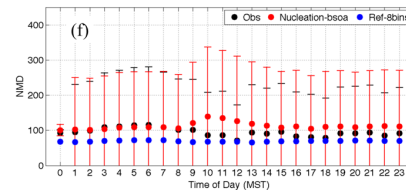
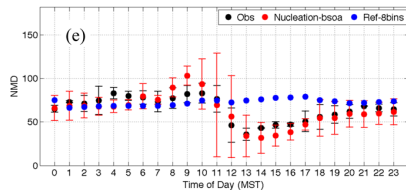
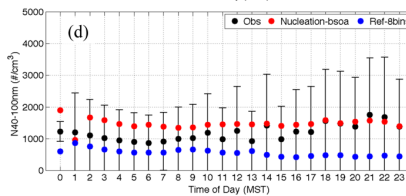
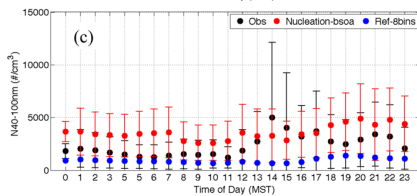
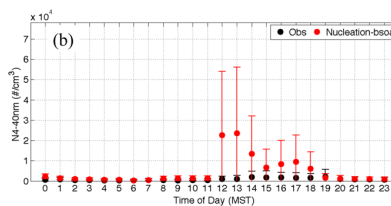
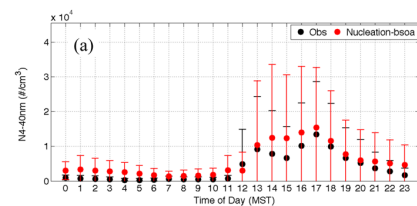


Fig. 4. Wind roses of local wind variations at 30 m height plotted by hours of day at MEFO from 06:00 to 18:00 MST during (a) APEs and (b) non-APE days. (c, d) Regional wind preferred directions corresponding to (a) and (b), respectively, based on WRF-FLEXPART analysis.

Modeling ultrafine particle growth

Y. Y. Cui et al.



Title Page

Abstract

Introduction

Conclusions

References

Tables

Figures

◀

▶

◀

▶

Back

Close

Full Screen / Esc

Printer-friendly Version

Interactive Discussion



Fig. 5. Comparison between measurements and simulations in diurnal profiles during APE days (left column) and Non-APE days (right column). Black dots are observations, red dots are simulations from Nucleation-bsoa run, and blue dots are simulations from Ref-8bins run. Error bars show 1σ variability. Plots show diurnal variations in **(a, b)** number concentrations of 4 to 40 nm particles ($N_{4-40\text{nm}}$) and **(c, d)** of 40 to 100 nm particles ($N_{40-100\text{nm}}$), diurnal profiles of **(e, f)** the number mean diameters (NMD), **(g, h)** Kappa values, and **(i, j)** number concentrations of CCN at 0.5% supersaturation.

Modeling ultrafine particle growth

Y. Y. Cui et al.

[Title Page](#)[Abstract](#)[Introduction](#)[Conclusions](#)[References](#)[Tables](#)[Figures](#)[I◀](#)[▶I](#)[◀](#)[▶](#)[Back](#)[Close](#)[Full Screen / Esc](#)[Printer-friendly Version](#)[Interactive Discussion](#)

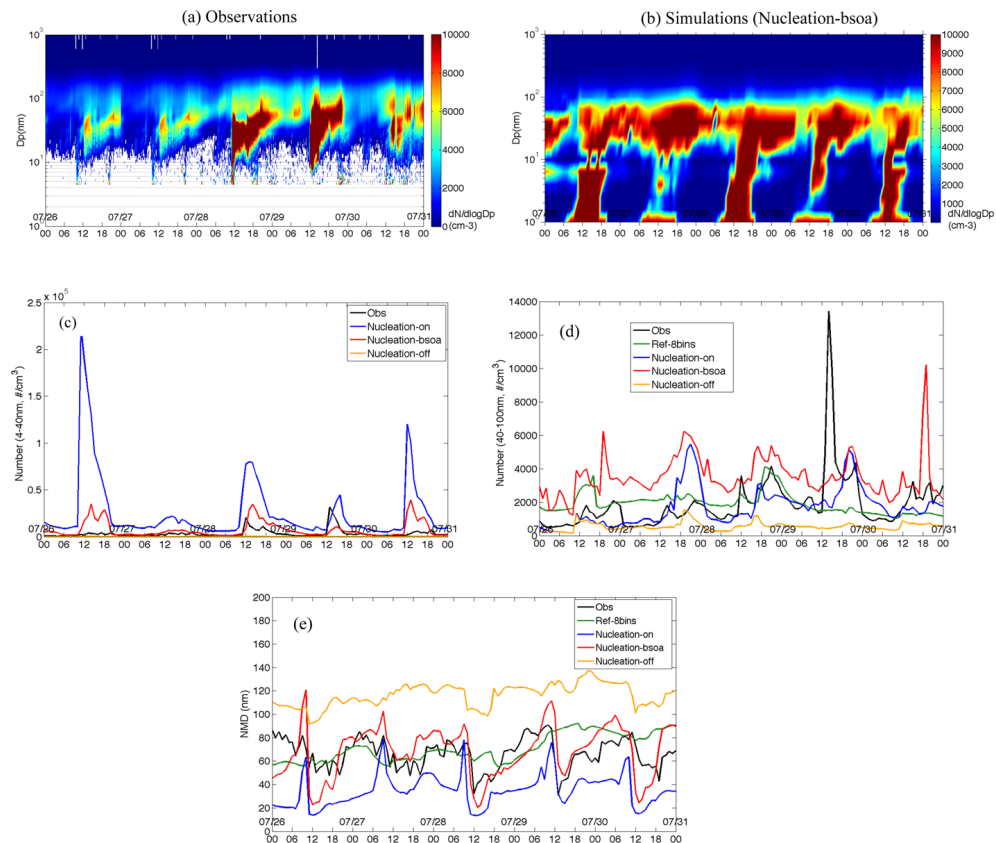


Fig. 6. Temporal evolution of the **(a)** observed and **(b)** simulated (Nucleation-bsoa) number size distributions, during 26–30 July 2011. Time series of number concentrations of particles in size ranges of **(c)** 4–40 nm and **(d)** 40–100 nm, and **(e)** number mean diameter (NMD, see Eq. 1) as observed and predicted at the MEFO site. Measurements are indicated by the black line (OBS), base case is green, Nucleation-on run is blue, “Nucleation-bsoa” is red, and Nucleation-off run is orange, respectively (see Table 2 for the model run descriptions).

[Title Page](#)
[Abstract](#)
[Introduction](#)
[Conclusions](#)
[References](#)
[Tables](#)
[Figures](#)
[◀](#)
[▶](#)
[◀](#)
[▶](#)
[Back](#)
[Close](#)
[Full Screen / Esc](#)
[Printer-friendly Version](#)
[Interactive Discussion](#)

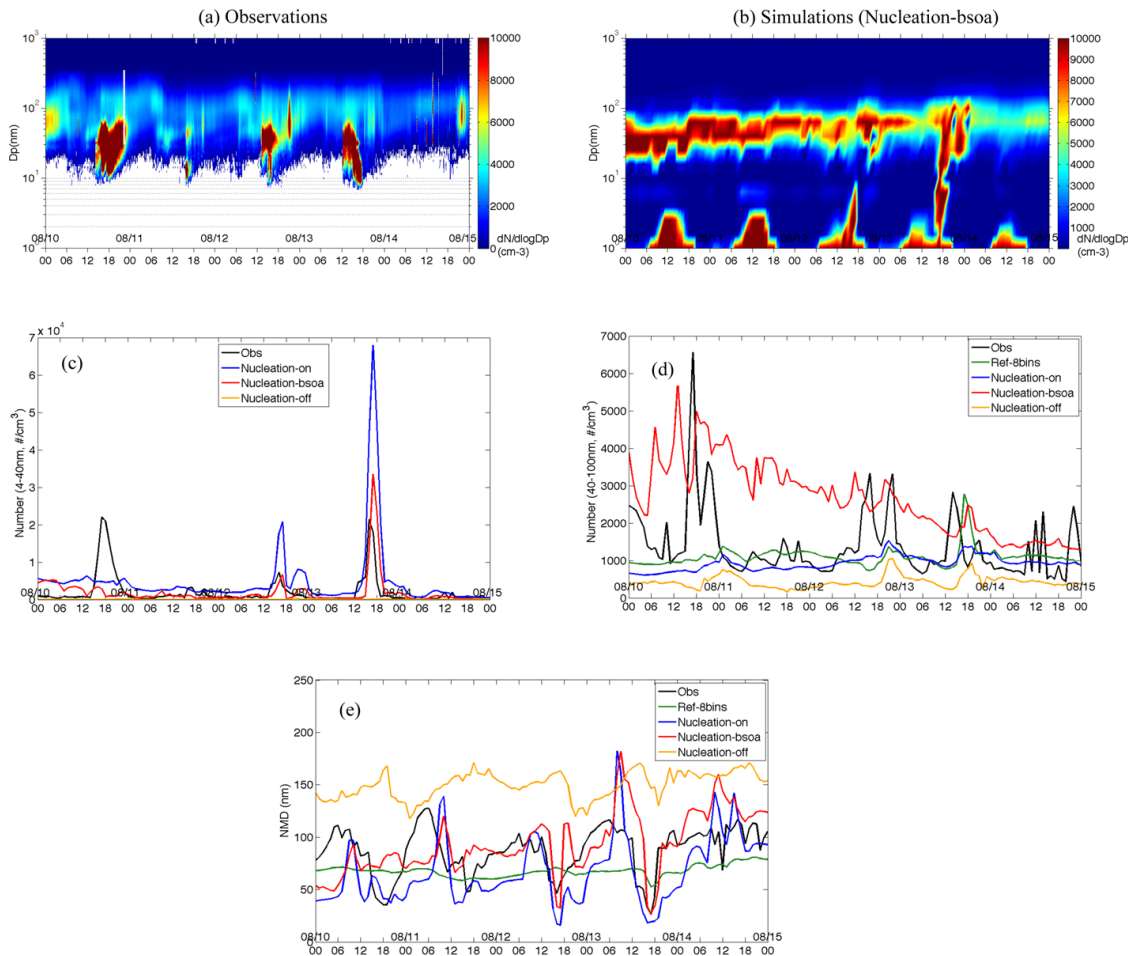



Fig. 7. Similar to Fig. 6 but for the 10–14 August 2011 time period.

Title Page

Abstract Introduction

Conclusions References

Tables Figures

◀ ▶

◀ ▶

Back Close

Full Screen / Esc

Printer-friendly Version

Interactive Discussion



Modeling ultrafine particle growth

Y. Y. Cui et al.

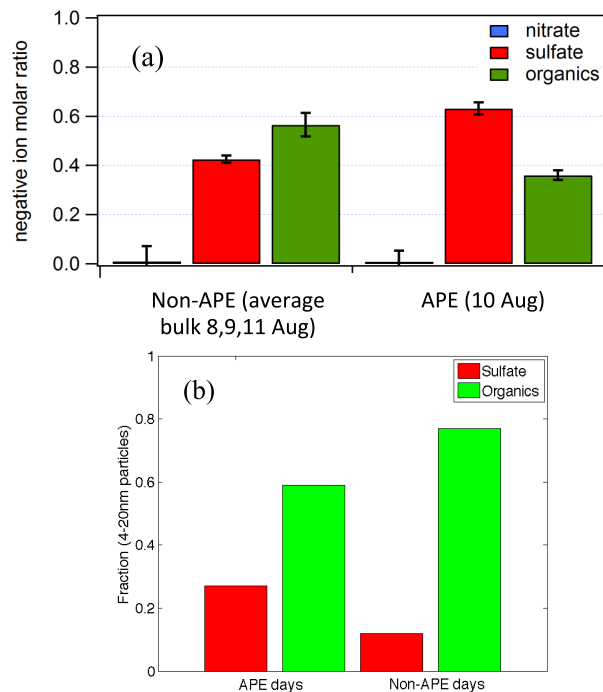


Fig. 8. (a) Comparison between bulk aerosol composition during 8–11 August excluding 10 August, and observed negative ion molar ratios of 20 nm particles on 10 August, using TDCIMS. **(b)** is composition fractions during predicted APE days and Non-APE days, here focused on July period.

Modeling ultrafine particle growth

Y. Y. Cui et al.

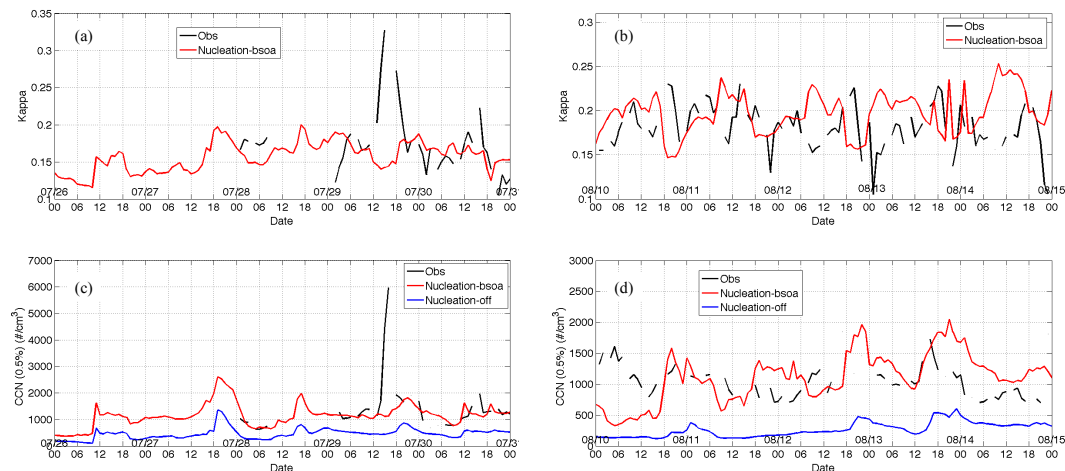


Fig. 9. Observed and predicted (Nucleation-bsoa) **(a, b)** volume-averaged hygroscopicity (κ) and **(c, d)** CCN concentrations at high supersaturation condition (0.5 %) from 26–31 July and 10–15 August 2011. The blue line shows the results without nucleation within PBL from “Nucleation-off” model run.

Title Page

Abstract

Introduction

Conclusions

References

Tables

Figures

◀

▶

◀

▶

Back

Close

Full Screen / Esc

Printer-friendly Version

Interactive Discussion

